

Vortex-vortex interactions in toroidally trapped Bose-Einstein condensates

T. Schulte, L. Santos, A. Sanpera and M. Lewenstein

Institut für Theoretische Physik, Universität Hannover, 30167 Hannover, Germany

(Dated: October 24, 2018)

We analyze the vortex dynamics and vortex–vortex interactions in Bose-Einstein condensates confined in toroidal traps. We show that this particular geometry strongly distorts the vortex dynamics. The numerically calculated vortex trajectories are well explained by an analytical calculation based on image method and conformal mapping. Finally, the dissipation effects are discussed.

Introduction

The realization of Bose-Einstein Condensation (BEC) in trapped dilute alkali gases [1, 2, 3, 4, 5, 6] has opened the possibility to explore fundamental effects of low temperature physics in a very controllable way. In this sense, several effects related to superfluidity [7] have been recently reported [8, 9]. Among the phenomena related to superfluidity, the possibility of observing vortices with quantized circulation [10] has aroused a big interest. Due to the diluteness of the atomic condensates, accurate theoretical predictions are possible. In addition, in these systems, the diameter of the vortex core is typically three orders of magnitude larger than for superfluid Helium, allowing for a more straightforward optical observation. Numerous theoretical schemes have been suggested for the generation of vortices in BEC, see e.g. Refs.[11, 12, 13, 14, 15, 16, 17]. So far only two techniques have successfully generated vortices in condensates, namely the stirring of a condensate with a blue detuned laser [18, 19], and the phase imprinting method achieved via the coherent interconversion between the two components of a binary condensate [20]. In addition the creation of a vortex ring after the decay of a dark soliton has been recently reported [21]. The dynamics and stability of vortices in trapped Bose-Einstein condensates has recently also been a subject of active investigation [22, 24, 25].

In the majority of current BEC experiments, the condensate is created in a cylindrical trap, either pancake-shaped, or cigar-shaped. However, in the recent years the possibility of creating a BEC in toroidal traps has aroused a growing interest. Toroidal traps have already been used in early Sodium BEC experiments at MIT [2], and in recent experiments on vortices at JILA [20]. Also, very recently the idea of creating a toroidal optical dipole trap using Laguerre-Gaussian beams has been proposed [26]. The physics of condensates in toroidal traps have been extensively investigated during the last recent years, including the ground state properties and elementary excitations [27, 28], the possibility to obtain vortices which due to the toroidal topology could be metastable beyond some critical nonlinearity [27, 28, 29, 30], the generation and properties of solitons and the so called "svortices" in this kind of traps [31], and even the possibility to obtain a mode-locked atom laser with toroidal geometry [32]. Very recently, we have proposed that a time-

averaged potential produced by the shaking of an usual Gaussian trap also leads to the formation of a double well or a toroidal condensate [33]. Additionally, if during the condensate shaking a proper phase is imprinted, dark solitons and eventually vortices can be created in a controllable way within the torus. In Ref. [33], it was already reported, that the particular toroidal geometry significantly modifies the vortex dynamics, as well as the vortex–vortex interaction. It is the aim of this paper to extend the analysis of Ref. [33]. We analyze in detail the effects of the geometry for toroidal box potentials, as well as those produced by the smooth transversal confinement. Interestingly, we show that the vortex dynamics obtained from direct numerical simulations can be analytically well described by means of the so-called image method, and conformal mapping techniques. Finally we analyze the vortex dynamics in presence of dissipation.

The structure of the paper is as follows. In Sec. I we describe the physical system, as well as the numerical techniques employed. In Sec. II we consider the case of a toroidal box potential, and introduce the image technique, as well as the corresponding conformal mapping, to analytically describe the vortex dynamics, as well as the vortex interaction. The case of a toroidal trap with harmonic transversal confinement is considered in Sec. III, where the effects caused by the smooth trapping potential are considered. Sec. IV is devoted to a brief discussion of the dissipation effects in the system. We finalize with some conclusions in Sec. V.

I. MODEL

At sufficiently low temperatures, the dynamics of a condensate in an external potential V can be well described by the so-called Gross-Pitaevskii equation [34, 35, 36]

$$i\hbar\frac{\partial\Psi}{\partial t} = -\frac{\hbar^2}{2m}\nabla^2\Psi + V\Psi + g|\Psi|^2\Psi, \quad (1)$$

where $g = \frac{4\pi\hbar^2 a N}{m}$ denotes the coupling constant, m refers to the atomic mass, a is the corresponding s -wave scattering length, and N is the number of condensed atoms. We shall consider in the present paper trapping potentials in which the condensate is strongly confined along one direction, so that the mean field energy is smaller than the excitation energy of the trap in

this direction. In this situation, the BEC can be considered as quasi-2D, and we can restrict ourselves to the analysis of the corresponding 2D GPE, with a modified coupling constant $g_{2D} = g \int dz |\psi(z)|^4$, where $\psi(z)$ is the wavefunction in the strongly confined z -direction. Both 2D [37] and quasi-2D [38, 39] BEC has been recently observed in experiments. The potential V in the remaining two dimensions has an annular shape, which we shall consider possessing rigid box boundaries in Sec. II, or harmonic transversal confinement in Sec. III. We restrict ourselves in the following to the situations in which the BEC can be considered in the Thomas-Fermi regime, i.e. the mean-field energy is much larger than the typical energy spacing of the annular trap. We consider in the following numerical simulations the case of $N = 10^5$ condensed Sodium atoms ($a = 2.75$ nm).

We perform the integration of equation (1) by an alternating direction implicit (ADI) Crank-Nicholson scheme [40], using cylindrical coordinates, due to the particular symmetry of the trapping potential. In the present paper, we shall not consider the issue of the experimental creation of the vortices, but rather we shall concentrate on the vortex dynamics once created. In order to numerically create the vortices, we employ the Crank-Nicholson procedure in imaginary time, while ensuring at each time step the proper phase pattern necessary to create the vortices [41]. This leads to the creation of vortex states, which are free of any other kind of excitation, and, therefore, allow for a clear analysis of the vortex dynamics. The proper phase pattern imprinted during the imaginary time evolution has to be carefully chosen. In particular, the boundary effects have to be taken into account in the method, by adding the corresponding phase contribution of the image vortices (see next section). Once the vortices are created we perform a real time evolution.

II. BOX-LIKE TOROIDAL TRAP

In this section, we investigate the evolution of vortex states in an annular trap with rigid boundaries. In such a trap the condensate density in the bulk is constant and shrinks to zero at the condensate boundaries on a length scale of the order of the healing length $\eta = 1/\sqrt{8\pi na}$, where n is the condensate density. Due to the absence of the potential in the interior of the torus and the homogeneity of the density inside the box, the vortex dynamics is completely determined by the toroidal geometry. In our numerical simulations we have considered a trap with inner rigid boundary at a radius $R_1 = 12\mu\text{m}$, and an outer one at $R_2 = 18\mu\text{m}$. We shall not consider, neither in this section nor in the next one, dissipation effects. These effects will be discussed in Sec. IV.

Single vortex dynamics

We consider first the situation in which a single vortex is placed in a toroidal trapped condensate. Due to the boundary effects the vortex will not remain at rest, but on the contrary it will move at a fixed radius around the torus, where the direction and the modulus of the vortex velocity depends on its circulation κ , and on the radial position at which it is created. In Fig. 1, we present the numerical results for the vortex velocity as a function of the radial vortex position.

Such dynamics can be well understood by employing the so-called image method [23, 24, 25]. Let us briefly review this method. In a homogeneous (untrapped) condensate the phase of a state containing a q times charged vortex is given by $e^{iq\varphi}$, where φ is the polar angle centered at the position of the vortex [42]. Therefore, the superfluid velocity becomes $\vec{v}_{SF} \equiv \hbar\nabla S/m = \hbar q/m\rho \vec{e}_\varphi$, where S is the condensate phase and ρ is the distance from the vortex line. In the following, we shall only discuss vortices with one quantum of circulation since, in the cases considered, vortices with $q > 1$ will decay into $q = 1$ vortices. For trapped condensates in the Thomas-Fermi regime, the hydrodynamic form of the Gross-Pitaevskii-equation allows to approximately impose for the superfluid velocity field the boundary condition of ordinary hydrodynamics, namely the vanishing of the normal component of the superfluid velocity field at the condensate boundary [43]. This boundary condition and the specification of the positions and circulations of the vortices, leads to the determination of the superfluid velocity field [23]. Moreover, the vortex dynamics in the homogeneous, and also in the boxlike trapped quantum gas, reproduces the classical vortex dynamics, which is governed by the Kelvin theorem, i.e. a vortex moves with the same velocity than the superfluid at its position [44]. This velocity can be calculated by employing a well-known method in classical hydrodynamics, namely the replacement of the boundaries by additional fictitious vortices, so called image vortices. These vortices must be placed at the appropriate positions with the appropriate circulations, such that the resulting velocity field obeys the boundary conditions for the considered geometry.

For the toroidal geometry in question, we have to take into account two (in principle infinite) families of image vortices. For the first family, an image vortex is placed at $\vec{r}_{im1} = \frac{R_1^2}{r} \frac{\vec{r}}{r}$ with circulation $-\kappa$ and one image vortex with circulation κ at the origin [45], where \vec{r} denotes the position vector of the real vortex in a frame centered at the origin of the torus [46]. The image vortex at \vec{r}_{im1} induces a velocity component normal on the outer circle, so in addition we need an image vortex at $\vec{r}_{im2} = \frac{R_2^2}{r_{im1}} \frac{\vec{r}}{r} = \frac{R_2^2}{R_1^2} \vec{r}$ with circulation κ . In turn this image will induce some normal component on the inner circle, so two more image vortices are required: one at $\vec{r}_{im3} = \frac{R_1^2}{r_{im2}} \frac{\vec{r}}{r} = \frac{R_1^4}{R_2^2 r} \frac{\vec{r}}{r}$ with circulation $-\kappa$ the other one at the origin with circulation κ and

so on and so forth. For the second family, one considers an image vortex at $\vec{r}'_{im1} = \frac{R_2^2}{r} \vec{r}$ with circulation $-\kappa$. This image vortex gives a normal component of the velocity on the inner circle so we need in addition one image vortex at $\vec{r}'_{im2} = \frac{R_1^2}{r_{im1}} \vec{r} = \frac{R_1^2}{R_2^2} \vec{r}$ with circulation κ as well as one image vortex at the origin with circulation $-\kappa$. For this we require another image vortex at $\vec{r}'_{im3} = \frac{R_2^2}{r'_{im2}} \vec{r} = \frac{R_2^4}{R_1^2 r} \vec{r}$ with circulation $-\kappa$ and so on.

The total superfluid velocity is made up by the contributions of all vortices (both real and image):

$$\vec{v}_{SF} = \sum_n q_n \frac{\hbar}{m} \vec{e}_z \times \frac{\vec{r} - \vec{r}_n}{|\vec{r} - \vec{r}_n|^2}. \quad (2)$$

In absence of friction, the superfluid velocity at the vortex position equals the velocity of the vortex line. Therefore we get for the vortex velocity:

$$\begin{aligned} 2\pi \frac{d}{dt} \vec{r} = & \sum_{n=1}^{\infty} \left(\frac{\kappa \left(r - r \left(\frac{R_2}{R_1} \right)^{2n} \right) \vec{e}_\varphi}{\left(\vec{r} - \left(\frac{R_2}{R_1} \right)^{2n} \vec{r} \right)^2} + R_1 \leftrightarrow R_2 \right) \\ & - \sum_{n=0}^{\infty} \left(\frac{\kappa \left(r \left(\frac{R_1}{R_2} \right)^{2n} \frac{R_1^2}{r} \right) \vec{e}_\varphi}{\left(\vec{r} - \left(\frac{R_1}{R_2} \right)^{2n} \frac{R_1^2}{r^2} \vec{r} \right)^2} + R_1 \leftrightarrow R_2 \right) \\ & + \frac{\kappa}{r} \vec{e}_\varphi. \end{aligned} \quad (3)$$

where $R_1 \leftrightarrow R_2$ denotes the same term as the precedent one, but with R_1 and R_2 interchanged. This velocity field is in good agreement with that calculated from our numerical simulations.

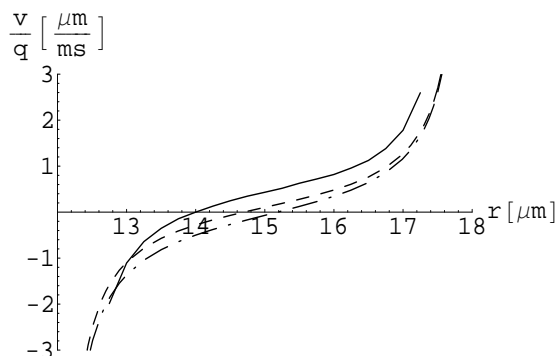


FIG. 1: Velocity of the vortex in a box like toroidal trap as a function of the radial coordinate. The three curves are obtained by direct evaluation of Eq. (3) (dashed), Eq. (21) (dashed-dotted) and by solving the GPE numerically (solid).

Vortex–vortex interaction

We can at this point analyze the vortex–vortex interaction within an annular trap with rigid boundaries. In a homogeneous condensate the vortex–vortex interaction depends on their relative circulation. In absence of dissipation, vortices with the same circulation orbit at a fixed distance from the central point between them. On the other hand, vortices with opposite circulation move parallel to each other forming a so-called vortex pair, which moves as a whole with a velocity which depends on the separation between the vortices. Two vortices in a toroidal box exhibit a completely different behavior. We shall consider in the following several possible scenarios.

Vortices with the same circulation created at different radii but at the same polar angle show a dynamics very similar to that of the homogeneous case: they perform deformed orbits around each other but with an overall drift around the torus (see. Fig. 2). On the contrary, vortices with opposite circulation created on the same radial coordinate, but at opposite positions in the torus show an interesting evolution, as already discussed in Ref. [33]. As shown in Fig. 3, the vortices move towards each other keeping the radial coordinate constant. When approaching, they move radially, and separate on a new constant radius, i.e. effectively they repel each other. When they meet at the other side of the torus, they repel each other again, and return to the original radial coordinate, i.e. the overall trajectory for each vortex is closed. If the vortex–anti vortex–pair is created such that the vortices are close to each other at the same polar angle, one vortex moves very quickly (during a few ms) towards the condensate boundary, where it is destroyed. The other one moves slightly, changes its initial radial position, and later on moves on a fixed radius (Fig. 4). This effect explains the results of Ref. [33], where a dark–soliton created in a toroidal geometry seemed to decay into just one vortex, apparently violating the conservation of the angular momentum. The dark–soliton actually decays into two vortices, but one of them is rapidly destroyed at the condensate boundary, while the remaining one is set into an orbit around the annulus.

Employing, as above, the image method technique, the

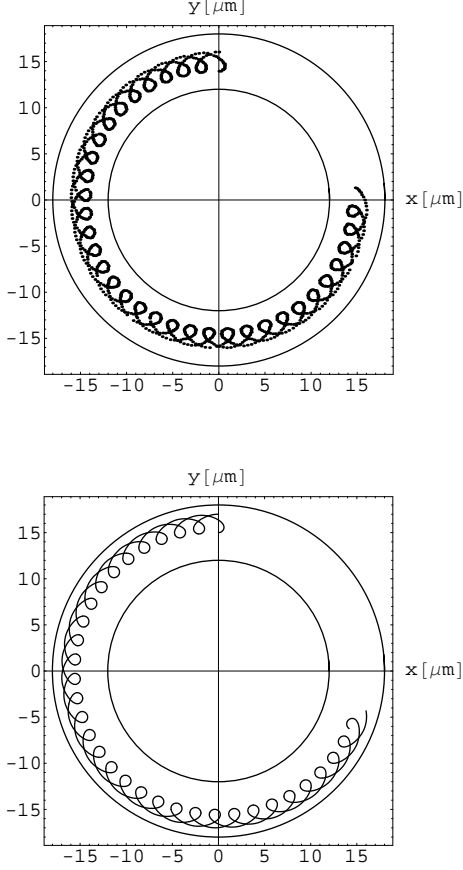


FIG. 2: (a) Trajectories of vortices with the same circulation created at different radii but on the same polar angle, obtained by solving the GPE numerically; (b) Results obtained using the image method.

equation for the position of the i -th vortex can be found:

$$\begin{aligned}
 2\pi \frac{d}{dt} \vec{r}_i = & \sum_{j=1}^2 \sum_{n=1}^{\infty} \left(\frac{\kappa_j \left(r_i \vec{e}_{\varphi_i} - r_j \left(\frac{R_2}{R_1} \right)^{2n} \vec{e}_{\varphi_j} \right)}{\left(\vec{r}_i - \left(\frac{R_2}{R_1} \right)^{2n} \vec{r}_j \right)^2} + R_1 \leftrightarrow R_2 \right) \\
 - & \sum_{j=1}^2 \sum_{n=0}^{\infty} \left(\frac{\kappa_j \left(r_i \vec{e}_{\varphi_i} - \left(\frac{R_1}{R_2} \right)^{2n} \frac{R_1^2}{r_j} \vec{e}_{\varphi_j} \right)}{\left(\vec{r}_i - \left(\frac{R_1}{R_2} \right)^{2n} \frac{R_1^2}{r_j} \vec{r}_j \right)^2} + R_1 \leftrightarrow R_2 \right) \\
 + & \frac{\kappa_{j \neq i} \left(r_i \vec{e}_{\varphi_i} - r_{j \neq i} \vec{e}_{\varphi_{j \neq i}} \right)}{\left(\vec{r}_i - \vec{r}_{j \neq i} \right)^2} + \sum_{j=1}^2 \frac{\kappa_j}{r_i} \vec{e}_{\varphi_i} \\
 & i, j = 1, 2.
 \end{aligned}$$

As observed in Figs. 2, 3, and 4), the results from Eq. (4) are in good agreement with the direct numerical sim-

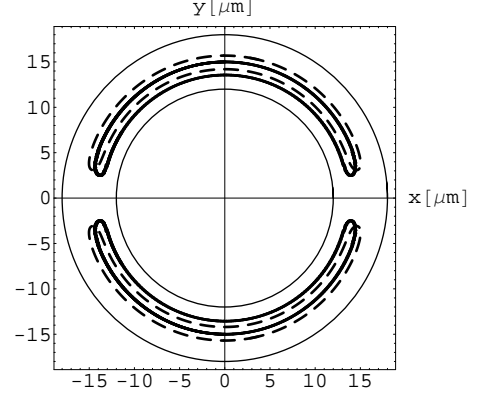


FIG. 3: Trajectories of a vortex-anti vortex pair. The vortices are initially created on the same radial distance but on opposing sides in the torus. We obtain the solid trajectories by solving the GPE numerically. The dashed trajectories are the computed solutions of the coupled differential equations (4). The period of oscillation for this setup is 225 ms.

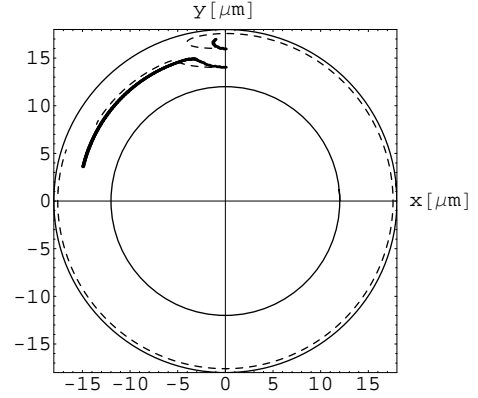


FIG. 4: Trajectories of a vortex-anti vortex pair. The vortices are initially created on the same polar angle but on different radii. One vortex moves to the condensate boundary, the other one stays in the torus. We obtain the solid trajectories by solving the GPE numerically. The dashed trajectories are the computed solutions of the coupled differential equations (4).

(4) ulations. Deviations from the numerical solutions of the GPE are basically due to deformations of the vortex core (see Sec. V), since the image method does not take into account the internal structure of the vortex core.

Analytical results. Conformal mapping.

In this section, we obtain the analytical expression of the vortex velocities explicitly, by employing a method which combines the previously presented image method and conformal mapping techniques [23].

Analytical method

We introduce a complex velocity potential $p(z = x + iy) = \phi(x, y) + i\gamma(x, y)$, such that $dp/dz = u - iw$ is the velocity $\vec{v} = (u, w)$. $p(z)$ has to be analytic everywhere except for singularities, and therefore $\phi(x, y)$ and $\gamma(x, y)$ are both solutions to the Laplace equation. One of them can be chosen to be the real velocity potential: $\nabla\phi = \vec{v}$. The curves $\phi = \text{constant}$ and $\gamma = \text{constant}$ intersect in right angles and correspond to the equipotential and stream lines. It can be easily seen, that

$$p(z) = -\frac{i\kappa}{2\pi} \log(z - z_j) \quad (5)$$

is the complex velocity potential of a single line vortex at position z_j , and consequently

$$\vec{v} = \frac{\kappa}{2\pi} \frac{1}{|\vec{r} - \vec{r}_j|} \vec{e}_{\varphi_j}. \quad (6)$$

In presence of rigid boundaries the velocity field is constrained to have a vanishing normal component at the boundaries and, therefore, since the flow is always in the direction of the stream lines, the boundaries correspond to curves of constant $\gamma(x, y)$. One can always arrange $p(z)$ such that this constant is zero, so one has $\text{Im}[p(z)] = 0$ for all z at the boundary, where Im indicates imaginary part. The potential $p(z)$ is constructed from the Green's function of the corresponding boundary value problem, by superposing the contribution of the N vortices to the flow [45]:

$$p(z) = f(z) + \sum_j^N \kappa_j G(z, z_j). \quad (7)$$

The term $f(z)$ allows for some further flow due to moving boundaries. The Green's function has the form $G(z, z_j) = \text{fund}(z, z_j) + g(z, z_j)$, where $\text{fund}(z, z_j)$ corresponds to the fundamental solution without any boundary (and also carries the divergence at the vortex positions). According to (5):

$$\text{fund}(z, z_j) = -\frac{i}{2\pi} \log(z - z_j). \quad (8)$$

The function $g(z, z_j)$ accounts for the constraints and it is smooth at the position of the vortices. It can be thought of as the complex potential induced by the images. Therefore, the velocity of the j -th vortex is given

by:

$$\begin{aligned} \kappa_j (u_j - iw_j) &= \kappa_j \frac{d}{dz} \left(p(z) - \text{fund}(z, z_j) \right) \Big|_{z=z_j} \\ &= \frac{\partial\psi}{\partial y_j} + i \frac{\partial\psi}{\partial x_j}, \end{aligned} \quad (9)$$

where we have employed the, so called, Kirchhoff-Routh function [45]

$$\psi \equiv \sum_{j=1}^N \kappa_j \text{Im} \left[f(z_j) + \sum_{\substack{k=1 \\ k \neq j}}^N \frac{\kappa_k}{2} G(z_j, z_k) + \frac{\kappa_j}{2} g(z_j, z_j) \right], \quad (10)$$

which is an integral of motion in the case of fixed boundaries. Note, that contrary to the situation considered in electrostatics, there is no contribution from $\text{fund}(z, z_j)$ at the position of the vortex, since a vortex (possessing cylindrical symmetry) does not act on itself.

For complicated geometries the velocity potential and the Kirchhoff-Routh function are difficult to calculate. In order to simplify one can map the complex plane which contains the complicated boundary value problem into another complex plane where the boundary geometry is simpler. A mapping $F(z)$, which carries the z -plane into the ζ -plane, $\zeta = F(z = x + iy) = s(x, y) + i t(x, y)$, is called conformal if $F(z)$ is, apart from isolated points, an analytic function of z , the inverse mapping $z = H(\zeta)$ exists, and $H(\zeta)$ is an analytic function of ζ . A conformal mapping maps continuous curves (in particular the boundaries) into continuous curves, and the solutions of the Laplace equation into solutions of the Laplace equation, i.e. if the boundary value problem in the original plane is fulfilled, then it is also fulfilled in the new plane with the new boundaries being the mappings of the original ones. The transformation behaviour under the conformal mapping:

$$\psi = \psi' + \sum_j \frac{\kappa_j^2}{4\pi} \ln \left| \frac{dH}{d\zeta} \Big|_{\zeta=\zeta_j} \right| \quad (11)$$

relates the Kirchhoff-Routh function of the old and new coordinates [45]. This transformation law can be deduced by the relation between the velocity of the j -th vortex in the z -plane and in the ζ -plane:

$$\begin{aligned} u_j - iw_j &= \frac{d\bar{z}_j}{dt} \\ &= \frac{d\bar{\zeta}_j}{dt} \frac{1}{(dH/d\zeta)|_{\zeta=\zeta_j}} + \frac{i\kappa_j}{4\pi} \frac{\frac{d^2 H}{d\zeta^2} \Big|_{\zeta=\zeta_j}}{\left((dH/d\zeta)|_{\zeta=\zeta_j} \right)^2}, \end{aligned} \quad (12)$$

where z_j and ζ_j denote the position of the j -th vortex in the corresponding coordinates and the bar denotes the complex conjugate.

One vortex in the torus

Let us first calculate the velocity of one vortex in the torus. As already shown, the image configuration is slightly complicated. Let us now assume that the torus is centered at the origin of the slitted complex z -plane with radii R_1 and R_2 respectively. The mapping:

$$\begin{aligned} F_1(z) = \zeta &= (2\pi - \theta) + i(\ln(r) - \ln(R_1)) \\ &= 2\pi + i \log z - i \ln R_1 \end{aligned} \quad (13)$$

with θ and r corresponding to the cylindrical coordinates of the z -plane, maps the annulus of the slitted z -plane onto a strip of width $b = \ln(R_2/R_1)$ and length 2π in the ζ -plane, since we consider here only the principal branch of the logarithm. The inverse mapping is

$$z = H_1(\zeta) = R_1 \exp(-i\zeta). \quad (14)$$

We approximate the velocity field in this strip of finite length by the velocity field in a strip of infinite length. This approximation obviously becomes better as $R_2/R_1 \rightarrow 1$. Let us consider a second conformal mapping

$$F_2(\zeta) = \xi = \exp\left(\frac{\pi}{b}\zeta\right), \quad H_2(\xi) = \zeta = \frac{b}{\pi} \log \xi \quad (15)$$

which maps the infinite strip to the upper half plane and the boundaries of the infinite strip in the ζ -plane onto the real axis in the ξ -plane. We denote the position of the vortex in the ζ -plane as ζ_1 and in the ξ -plane as ξ_1 . In the ξ -plane it is sufficient to consider one image vortex at position $\bar{\xi}_1$ to fulfill the boundary condition. The complex velocity potential in the ξ -plane is therefore given by

$$P(\xi) = -\frac{i\kappa}{2\pi} \log(\xi - \xi_1) + \frac{i\kappa}{2\pi} \log(\xi - \bar{\xi}_1). \quad (16)$$

The velocity of the vortex in the ξ -plane is:

$$\begin{aligned} U_1^\xi - iW_1^\xi &= \frac{d\bar{\xi}_1}{dt} = \frac{d}{d\xi} \left[P(\xi) + \frac{i\kappa}{2\pi} \log[\xi - \xi_1] \right] \Big|_{\xi=\xi_1} \\ &= \frac{i\kappa}{2\pi} \frac{1}{\xi_1 - \bar{\xi}_1}. \end{aligned} \quad (17)$$

According to (12) we calculate the velocity of the vortex in the ζ -plane as:

$$U_1^\zeta - iW_1^\zeta = \frac{\kappa}{4b} \cot\left[\frac{\pi}{b}t_1\right]. \quad (18)$$

From this equation the Kirchhoff-Routh function in the ζ -plane can be obtained by solving (9):

$$\psi^\zeta(t_1) = \frac{\kappa^2}{4\pi} \ln \left[\sin \left(\frac{\pi}{\ln \frac{R_2}{R_1}} t_1 \right) \right], \quad (19)$$

where the ζ denotes that this is the Kirchhoff-Routh function for the ζ -plane. From the transformation law (11)

we get the Kirchhoff-Routh function of the original z -coordinates:

$$\psi(z_1) = \frac{\kappa^2}{4\pi} \ln \left[\sin \left(\frac{\pi}{\ln \frac{R_2}{R_1}} \ln \left(\frac{r_1}{R_1} \right) \right) \right] + \frac{\kappa^2}{4\pi} \ln(r_1). \quad (20)$$

And from (9) we obtain the vortex velocity:

$$\vec{v} = -\frac{\kappa}{4r \ln \frac{R_2}{R_1}} \cot \left(\frac{\pi}{\ln \frac{R_2}{R_1}} \ln \left(\frac{r}{R_1} \right) \right) \vec{e}_\varphi - \frac{\kappa}{4\pi r} \vec{e}_\varphi. \quad (21)$$

This analytical result is compared in Fig. 1 with the results obtained from the direct summation provided by the image method. The agreement is, as observed, excellent.

Two vortices in the torus

Let us now consider two vortices in the torus. We calculate first the velocity of the j -th vortex in an infinite strip of width b , containing two vortices. After applying again the mapping (15), and following the same notation as in the previous section, the complex potential in the new coordinates is made up of the contributions of the two real vortices and two image vortices:

$$P(\xi) = \frac{i\kappa_1}{2\pi} \log \left(\frac{\xi - \bar{\xi}_1}{\xi - \xi_1} \right) + \frac{i\kappa_2}{2\pi} \log \left(\frac{\xi - \bar{\xi}_2}{\xi - \xi_2} \right). \quad (22)$$

The velocity of the vortex 1 in the ξ -plane is given by:

$$U_1^\xi - iW_1^\xi = \frac{i\kappa_1/2\pi}{\xi_1 - \bar{\xi}_1} + \frac{i\kappa_2/2\pi}{\xi_1 - \bar{\xi}_2} - \frac{i\kappa_2/2\pi}{\xi_1 - \xi_2} \quad (23)$$

According to (12) we calculate the velocity of the vortex in the ζ -plane. After elementary but tedious calculations we obtain:

$$\begin{aligned} U_1^\zeta - iW_1^\zeta &= \frac{\kappa_1}{4b} \cot \left(\frac{\pi}{b} t_1 \right) \\ &+ \frac{\kappa_2}{4b} \left[\frac{\sin \left(\frac{\pi}{b} (t_1 + t_2) \right)}{\cosh \left(\frac{\pi}{b} (s_1 - s_2) \right) - \cos \left(\frac{\pi}{b} (t_1 + t_2) \right)} \right. \\ &+ \frac{\sin \left(\frac{\pi}{b} (t_2 - t_1) \right)}{\cosh \left(\frac{\pi}{b} (s_1 - s_2) \right) - \cos \left(\frac{\pi}{b} (t_2 - t_1) \right)} \\ &- i \frac{\sinh \left(\frac{\pi}{b} (s_1 - s_2) \right)}{\cosh \left(\frac{\pi}{b} (s_1 - s_2) \right) - \cos \left(\frac{\pi}{b} (t_2 - t_1) \right)} \\ &\left. + i \frac{\sinh \left(\frac{\pi}{b} (s_1 - s_2) \right)}{\cosh \left(\frac{\pi}{b} (s_1 - s_2) \right) - \cos \left(\frac{\pi}{b} (t_1 + t_2) \right)} \right]. \end{aligned} \quad (24)$$

For the second vortex, we have just to interchange the indices 1 and 2. From (9) we obtain the Kirchhoff-Routh

function:

$$\begin{aligned} \psi^\zeta = & \sum_{j=1}^2 \frac{\kappa_j^2}{4\pi} \ln \left(\sin \left(\frac{\pi}{b} t_j \right) \right) \\ & - \frac{\kappa_1 \kappa_2}{4\pi} \ln \left[\cos \left(\frac{\pi}{b} (t_1 - t_2) \right) - \cosh \left(\frac{\pi}{b} (s_1 - s_2) \right) \right] \\ & + \frac{\kappa_1 \kappa_2}{4\pi} \ln \left[\cos \left(\frac{\pi}{b} (t_1 + t_2) \right) - \cosh \left(\frac{\pi}{b} (s_1 - s_2) \right) \right], \end{aligned} \quad (25)$$

and from (11) the Kirchhoff-Routh function for the original z-plane, corresponding to two vortices in the torus:

$$\begin{aligned} \psi = & \sum_{j=1}^2 \frac{\kappa_j^2}{4\pi} \ln \left(\sin \left(\frac{\pi}{b} \ln \frac{r_j}{R_1} \right) \right) + \sum_{j=1}^2 \frac{\kappa_j^2}{4\pi} \ln (r_j) \\ & - \frac{\kappa_1 \kappa_2}{4\pi} \ln \left[\cos \left(\frac{\pi}{b} \ln \left(\frac{r_1}{r_2} \right) \right) - \cosh \left(\frac{\pi}{b} (\theta_1 - \theta_2) \right) \right] \\ & + \frac{\kappa_1 \kappa_2}{4\pi} \ln \left[\cos \left(\frac{\pi}{b} \ln \left(\frac{r_1 r_2}{R_1^2} \right) \right) - \cosh \left(\frac{\pi}{b} (\theta_1 - \theta_2) \right) \right]. \end{aligned} \quad (26)$$

Since the Kirchhoff-Routh function is for fixed boundaries a constant of motion, we obtain from this equation information about the vortex trajectories by computing the hyper surface on which the Kirchhoff function is conserved. In particular we investigate the case of the vortex-antivortex pair, where the vortices are initially placed on the same radial coordinate. Due to symmetry considerations it is clear, that the vortices will always stay on the same radial coordinates $r_1 = r_2$ and with this knowledge it is easy to compute the vortex trajectory

as curves of constant Kirchhoff-Routh function (see Fig. 5).

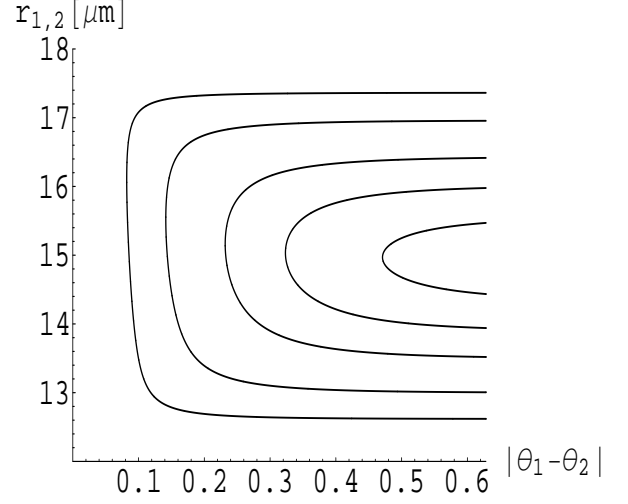


FIG. 5: Trajectories of a vortex-antivortex pair with vortices placed on the same radial coordinate. On the curves shown the Kirchhoff-Routh function is conserved. The vortices approach, move in radial direction and separate again (see FIG. 3). The asymmetry of the image configuration is responsible for the fact, that the trajectories are not symmetric with respect to reflection at $r = 15\mu\text{m}$.

From the Kirchhoff-Routh function we get the velocity of the j -th vortex:

$$\begin{aligned} \vec{v}_i = & \frac{1}{4 \ln \left(\frac{R_2}{R_1} \right) r_i} \left[\kappa_j \frac{\sin \left(\frac{\pi}{\ln \left(\frac{R_2}{R_1} \right) \ln \left(\frac{r_i r_j}{R_1^2} \right)} \right)}{\cos \left(\frac{\pi}{\ln \left(\frac{R_2}{R_1} \right) \ln \left(\frac{r_i r_j}{R_1^2} \right)} \right) - \cosh \left(\frac{\pi}{\ln \left(\frac{R_2}{R_1} \right)} (\theta_i - \theta_j) \right)} - \kappa_i \cot \left(\frac{\pi}{\ln \left(\frac{R_2}{R_1} \right)} \ln \left(\frac{r_i}{R_1} \right) \right) \right. \\ & \left. - \kappa_j \frac{\sin \left(\frac{\pi}{\ln \left(\frac{R_2}{R_1} \right) \ln \left(\frac{r_i}{r_j} \right)} \right)}{\cos \left(\frac{\pi}{\ln \left(\frac{R_2}{R_1} \right) \ln \left(\frac{r_i}{r_j} \right)} \right) - \cosh \left(\frac{\pi}{\ln \left(\frac{R_2}{R_1} \right)} (\theta_i - \theta_j) \right)} - \frac{\kappa_i}{\pi} \ln \left(\frac{R_2}{R_1} \right) \right] \vec{e}_{\varphi_i} \\ & + \frac{1}{4 \ln \left(\frac{R_2}{R_1} \right) r_i} \left[\kappa_j \frac{\sinh \left(\frac{\pi}{\ln \left(\frac{R_2}{R_1} \right)} (\theta_i - \theta_j) \right)}{\cos \left(\frac{\pi}{\ln \left(\frac{R_2}{R_1} \right) \ln \left(\frac{r_i}{r_j} \right)} \right) - \cosh \left(\frac{\pi}{\ln \left(\frac{R_2}{R_1} \right)} (\theta_i - \theta_j) \right)} \right. \\ & \left. - \kappa_j \frac{\sinh \left(\frac{\pi}{\ln \left(\frac{R_2}{R_1} \right)} (\theta_i - \theta_j) \right)}{\cos \left(\frac{\pi}{\ln \left(\frac{R_2}{R_1} \right) \ln \left(\frac{r_i r_j}{R_1^2} \right)} \right) - \cosh \left(\frac{\pi}{\ln \left(\frac{R_2}{R_1} \right)} (\theta_i - \theta_j) \right)} \right] \vec{e}_{r_i} \end{aligned} \quad (27)$$

with $i, j = 1, 2$, where $i \neq j$. In this formula one has to take into account, that the azimuthal separation between the vortices fulfills $|\theta_i - \theta_j| \leq \pi$. We have numerically solved the first-order differential equations resulting from this velocity field, and obtained the vortex trajectories, whose shapes are practically indistinguishable from the ones we obtain by numerically solving (4).

III. HARMONIC TOROIDAL TRAP

We discuss now the dynamics of vortices in a toroidal geometry with harmonic trapping in the radial direction:

$$V_{trap}(\vec{r}) = \frac{1}{2}m (\omega_\rho^2(\rho - \rho_0)^2 + \omega_z^2 z^2). \quad (28)$$

As before we consider a quasi-2D condensate in the Thomas-Fermi-Regime. In order to compare with the previous calculation for a box-like annulus, the trapping frequencies are adjusted such that the Thomas-Fermi radii correspond to an annular condensate with inner radius of $12\mu m$ and outer radius of $18\mu m$. The qualitative dynamic of the vortices is unchanged from that in the box-like case, but the time scales are different. Due to the inhomogeneity of the trapping potential a vortex will no longer only move with the superfluid velocity. In addition it will have some velocity with respect to the superfluid, resulting from the small deviation from the cylindrical symmetric vortex state caused by the potential.

This velocity can be calculated by the method of matched asymptotic expansion [47, 48], consisting in evaluating the form of the solution of equation (1) in the vortex core and far away from it. The vortex velocity can be calculated by the requirement that the asymptotic behavior of the two solutions has to coincide at a distance of the order of the healing length from the center of the vortex. The calculation yields [48]:

$$\vec{v}(\vec{r}_0) = -\frac{q\hbar}{2m} \left(\frac{\vec{e}_z \times \nabla V_{trap}(\vec{r}_0)}{g|\Psi_{TF}|^2} \right) \ln \left(\eta \sqrt{\frac{\nabla^2 V_{trap}}{4g|\Psi_{TF}|^2}} \right), \quad (29)$$

where \vec{r}_0 denotes the position of the vortex and Ψ_{TF} is the Thomas-Fermi wave function. Since the deviation from the cylindrical symmetric vortex solution in the smooth potential is small, we neglect completely their effect on the velocity field induced by the vortex. Therefore, we can employ again the image method for determining the velocity field fulfilling the boundary conditions. Therefore, the total velocity field results from adding to the field calculated in the previous section that of (29). This produces a very good agreement with our numerical results, as observed in Fig. 6.

The influence of the potential on the vortex velocity gives the possibility to control and manipulate the vortex dynamics by adiabatically changing the trapping potential. For instance, it is possible to reverse the direction of

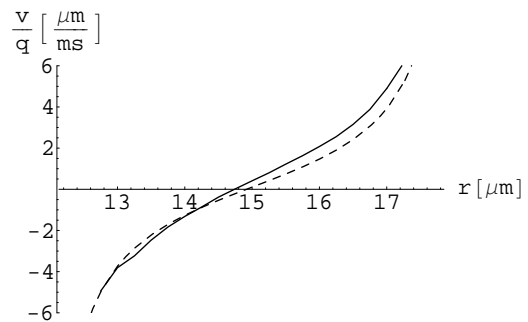


FIG. 6: Velocity of one vortex in the harmonic toroidal trap as a function of the radial coordinate. The solid curve shows the result of the numerical computation of the GPE, the dashed curve shows the combination of Eqs. (21) and (29).

the vortex orbit in the annular trap (Fig. 7). Let us consider the above investigated boxlike toroidal trap, where we create one vortex. If one imposes a slowly increasing linear slope on the initially flat ground of the box the contribution of (29) eventually becomes more important than the boundary effects, and the vortex turns backwards.

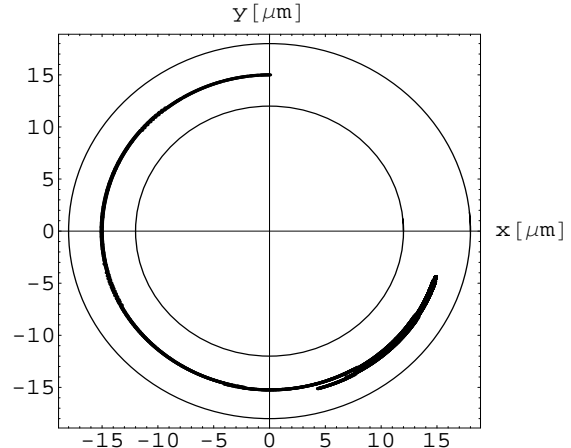


FIG. 7: Trajectory of one vortex in a box like toroidal trap obtained by numerical solution of the GPE. We add to the initially flat box like trap a linear, slowly increasing, slope. The vortex slows down as the slope increases and finally turns.

The vortex-vortex interaction is also affected by the transversal harmonic potential, but the qualitative behavior described in Sec. II is maintained [33].

IV. DISSIPATION EFFECTS

In this section, we discuss how dissipation affects the vortex dynamics in a toroidal geometry. Following a similar analysis as in Ref. [28, 41] we evaluate the free energy functional

$$E = \int d^3\mathbf{r} \left\{ \frac{\hbar^2}{2m} |\nabla\psi(\mathbf{r})|^2 + V(\mathbf{r})|\psi(\mathbf{r})|^2 + \frac{g}{2} |\psi(\mathbf{r})|^4 \right\} \quad (30)$$

for a condensate containing a vortex-anti-vortex pair with cylindrically symmetric vortex cores, for the vortex lines placed at the same radial coordinate r , but at different angles Θ_1, Θ_2 (see Fig. 8). Since the GPE describes a Hamiltonian evolution and it does not include any dissipation, the trajectories of the vortices according to the GPE are curves of constant energy. However, if the vortices approach each other (or the boundaries) to a distance comparable to the healing length, the vortex cores deform and the trajectories we obtain numerically slightly differ from these energy lines. The total energy increases with increasing distance between the vortices, or between a vortex and the torus boundaries, because the kinetic energy grows rapidly in this case. Therefore, we expect that in presence of dissipation, the vortices will tend to move towards the trap walls [24]. In addition, the vortices will tend to reduce the distance between each other, and therefore, if the vortices do not collide with the walls, the apparent repulsion introduced by the toroidal geometry will be eventually overcome, and the vortices will eventually collide, and mutually annihilate, as in homogeneous condensates.

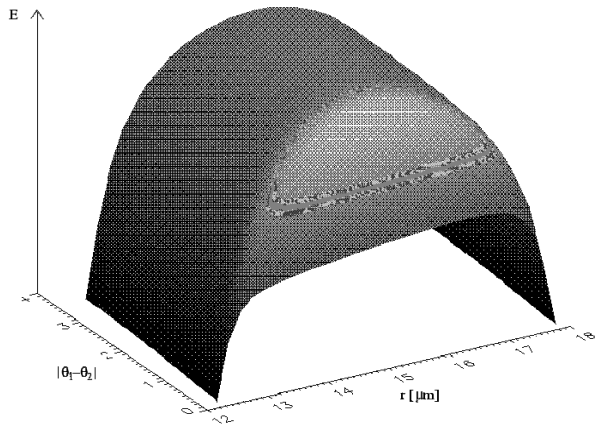


FIG. 8: Free energy of the condensate containing a vortex-antivortex-pair, depending on the positions of the vortices.

V. CONCLUSIONS AND OUTLOOK

In this paper, we have investigated the vortex dynamics and vortex-vortex interaction in an annular trapping

geometry. The vortex trajectories in the presence of rigid boundaries have been obtained numerically by direct numerical computation of the corresponding 2D GPE. We have shown that these trajectories can be well described by closed analytical formulas, obtained from the combination of the image method and conformal mapping. Additionally, we have considered the case of harmonic transversal confinement, and showed that the numerical results are in excellent agreement with the analytical ones, once included the effects of the inhomogeneous trapping potential calculated from the corresponding matched asymptotic expansion.

We should note at this point, that the image method is applicable, when the vortices are spatially separated by a distance greater than their core size, which is of the order of the healing length. The latter statement also concerns the distance between the vortices and the boundaries. If this is the case, no deformation of the vortex core is produced. However, if the vortices approach to distances comparable to the core size, the initially cylindrical symmetric vortex cores experience evident deformations and therefore, the results provided by the image method begin to depart from the numerically obtained ones. Similarly, the dynamics of vortices in the quantum gas begin to differ significantly from the classical theory [44, 49].

The analysis of the vortex dynamics has been limited to the case of 2D traps. Lower dimensional condensates are currently actively investigated, and very recently the experimental observation of 2D (and even 1D) condensates have been reported [37, 38, 39]. However, the results of the present paper and Ref. [33], open interesting questions concerning the behavior of vortices in 3D toroidal condensates. Preliminary results concerning vortex lines parallel to the torus axis, confirm that in a 3D torus an essentially similar picture as that discussed for 2D is obtained. However tiltings with respect to the torus axis, together with boundary effects, could lead to a significant bending of the vortex lines. This effect will affect the observability of the vortices, since the density minimum will depart from the direction of experimental observation. In addition, the bending will significantly distort the vortex dynamics, introducing an additional radial velocity to the vortex line. The vortex-vortex interaction is also expected to be significantly affected in the presence of a significant bending. The analysis of these effects, as well as those related with the propagation and interaction of vortex rings in toroidal geometries will be the subject of further investigation.

Acknowledgments

We acknowledge support from Deutsche Forschungsgemeinschaft (SFB 407), TMR ERBXTCT-96-002, and ESF PESC BEC2000+. L. S. wishes to thank the Alexander von Humboldt Foundation, the Federal Ministry of Education and Research and the ZIP Programme of the German Government. Discussions with K.-A. Suominen

and J.P. Martikainen are acknowledged.

-
- [1] M. H. Anderson, J. R. Ensher, M. R. Matthews, C. E. Wieman and E. A. Cornell, *Science* **269**, 198 (1995);
- [2] K.B. Davis, M. O. Mewes, M. R. Andrews, N. J. van Druten, D. S. Durfee, D. M. Kurn and W. Ketterle, *Phys. Rev. Lett.* **75**, 3969 (1995);
- [3] C. C. Bradley, C. A. Sackett, and R. G. Hulet, *Phys. Rev. Lett.* **78**, 985 (1997).
- [4] D. G. Fried, T. C. Killian, L. Willmann, D. Landhuis, S. C. Moss, D. Kleppner, and T. J. Greytak, *Phys. Rev. Lett.* **81**, 3811 (1998).
- [5] S. L. Cornish, N. R. Claussen, J. L. Roberts, E. A. Cornell, and C. E. Wieman, *Phys. Rev. Lett.* **85**, 1795 (2000).
- [6] A. Robert, O. Sirjean, A. Browaeys, J. Poupard, S. Nowak, D. Boiron, C. I. Westbrook, and A. Aspect, *Science* **292**, 461 (2001); F. Pereira Dos Santos, J. Léonard, Junmin Wang, C. J. Barrelet, F. Perales, E. Rasel, C. S. Unnikrishnan, M. Leduc, and C. Cohen-Tannoudji, *Phys. Rev. Lett.* **86**, 3459 (2001).
- [7] See e.g. E. M. Lifshitz and L. P. Pitaevskii, *Statistical Physics, Part 2*, (Pergamon Press, Oxford, U.K., 1980).
- [8] O. M. Moragò, S. A. Hopkins, J. Arlt, E. Hodby, G. Hechenblaikner, and C. J. Foot, *Phys. Rev. Lett.* **84**, 2056 (2000).
- [9] R. Onofrio, C. Raman, J. M. Vogels, J. R. Abo-Shaeer, A. P. Chikkatur, and W. Ketterle, *Phys. Rev. Lett.* **85**, 2228 (2000)
- [10] See e.g., R. J. Donnelly, *Quantized Vortices In Helium II* (Cambridge University Press, Cambridge, U.K., 1991).
- [11] K.-P. Martzlin, W. Zhang, and E. M. Wright, *Phys. Rev. Lett.* **79**, 4728 (1997); K.-P. Martzlin and W. Zhang, *Phys. Rev. A* **57**, 3801 (1998); *ibid.*, 4761 (1998).
- [12] R. Dum, J. I. Cirac, M. Lewenstein, and P. Zoller, *Phys. Rev. Lett.* **80**, 2972 (1998).
- [13] B. Jackson, J. F. McCann, and C. S. Adams, *Phys. Rev. Lett.* **80**, 3903 (1998).
- [14] B. M. Caradoc-Davies, R. J. Ballagh, and K. Burnett, *Phys. Rev. Lett.* **83**, 895 (1999).
- [15] L. Dobrek, M. Gajda, M. Lewenstein, K. Sengstock, G. Birkl, and W. Ertmer, *Phys. Rev. A* **60**, R3381 (1999).
- [16] J. Williams and M. Holland, *Nature* **401**, 568 (1999).
- [17] D. L. Feder, C. W. Clark, and B. I. Schneider, *Phys. Rev. A* **61**, 011601 (2000).
- [18] K. W. Madison, F. Chevy, W. Wohlleben, and J. Dalibard, *Phys. Rev. Lett.* **84**, 806 (2000); F. Chevy, K. W. Madison, J. Dalibard, *Phys. Rev. Lett.* **85**, 2223 (2000)
- [19] J. R. Abo-Shaeer, C. Raman, J. M. Vogels, and W. Ketterle, *Science* **292**, 476 (2001).
- [20] M. R. Matthews, B. P. Anderson, P. C. Haljan, D. S. Hall, C. E. Wieman, and E. A. Cornell, *Phys. Rev. Lett.* **83**, 2498 (1999).
- [21] B. P. Anderson, P. C. Haljan, C. A. Regal, D. L. Feder, L. A. Collins, C. W. Clark, and E. A. Cornell, *Phys. Rev. Lett.* **86**, 2926 (2001).
- [22] See e.g., A. L. Fetter and A. A. Svidzinsky, *J. Phys.: Condens. Matter* **13**, R135 (2001), and references therein.
- [23] G. K. Batchelor, *An introduction to fluid mechanics*, (Cambridge University Press, Cambridge, U.K., 1967)
- [24] P. O. Fedichev and G. V. Shlyapnikov, *Phys. Rev. A* **60**, R1779 (1999).
- [25] M. Guilleumas, and R. Graham, *Phys. Rev. A* **64**, 033607 (2001).
- [26] E. M. Wright, J. Arlt, and K. Dholakia, *Phys. Rev. A* **63**, 013608 (2000).
- [27] D. S. Rokhsar, cond-mat/9709212.
- [28] L. Salasnich, A. Parola, and L. Reatto, *Phys. Rev. A* **59**, 2990 (1999).
- [29] M. Benakli, S. Raghavan, A. Smerzi, S. Fantoni, and S. R. Shenoy, *Europhys. Lett.* **46**, 275 (1999).
- [30] J. Tempere, J. T. Devreese, and E. R. I. Abraham, *Phys. Rev. A* **64**, 023603 (2001).
- [31] J. Brand, and W. P. Reinhardt, *J. Phys. B: At. Mol. Opt. Phys.* **34**, L113 (2001).
- [32] P. D. Drummond, A. Eleftheriou, K. Huang, and K. V. Kheruntsyan, *Phys. Rev. A* **63**, 053602 (2001).
- [33] J. P. Martikainen, K. A. Suominen, L. Santos, T. Schulte, and A. Sanpera, *Phys. Rev. A* in press.; R. Dum, A. Sanpera, K.-A. Suominen, M. Brewczyk, M. Kus, K. Rzazewski and M. Lewenstein, *Phys. Rev. Lett.* **80**, 3899 (1998)
- [34] E. P. Gross, *Nuovo Cimento* **20**, 454 (1961)
- [35] E. P. Gross, *J. Math. Phys.* **4**, 195 (1963)
- [36] L. P. Pitaevskii, *Zh. Eksp. Teor. Fiz.* **40**, 646 (1961) [*Sov. Phys. JETP*, **13**, 451 (1961)]
- [37] A. I. Safonov, S. A. Vasilyev, I. S. Yasnikov, I. I. Lukashovich, and S. Jaakkola, *Phys. Rev. Lett.* **81**, 4545 (1998).
- [38] A. Gorlitz, J.M. Vogels, A.E. Leanhardt, C. Raman, T.L. Gustavson, J.R. Abo-Shaeer, A.P. Chikkatur, S. Gupta, S. Inouye, T.P. Rosenband, D.E. Pritchard, and W. Ketterle, cond-mat/0104549.
- [39] S. Burger, F. S. Cataliotti, C. Fort, P. Maddaloni, F. Minardi, and M. Inguscio, cond-mat/0108037.
- [40] W. H. Press et al., *Numerical Recipes*, Cambridge University Press, 1986
- [41] S. A. McGee and M. J. Holland, *Phys. Rev. A* **63**, 043608 (2001).
- [42] A. L. Fetter and A. A. Svidzinsky, *J. Phys.: Condens. Matter* **13**, R135 (2001)
- [43] E. Lundh and P. Ao, *Phys. Rev. A* **61**, 063612 (2000) and references therein.
- [44] A. L. Fetter, *Phys. Rev.* **151**, 100 (1966)
- [45] P. G. Saffman, *Vortex Dynamics*, (Cambridge University Press, 1992).
- [46] Since we are dealing with a multiple connected region, the velocity field is not determined uniquely by the boundary condition and the specification of the vorticity field alone. This is reflected by the fact that the vortex centered at the origin can have arbitrary circulation without affecting the boundary condition. We choose the central vortex to have the circulation stated in the text, to prevent ring currents. Fixing in that way the circulation of the vortex at the origin, sets the so-called cyclic constant of the velocity field to zero. With this additional information the velocity field is determined uniquely [23].
- [47] B. Y. Rubinstein and L. M. Pismen, *Physica D* **78**, 1 (1994).

- [48] A. A. Svidzinsky and A. L. Fetter, Phys. Rev. A **62**, 063617 (2000). [49] A. L. Fetter, Phys. Rev. **138**, 429 (1965)